Received: 16 September 2023 | Revised: 10 November 2023 | Accepted: 14 November 2023

DOI: 10.1002/jbio.202300384

RESEARCH ARTICLE

JOURNAL OF BIOPHOTONICS

A multimodal nonlinear optical microscopy study of the responses of *Pseudomonas aeruginosa* to blue light and antibiotic treatment

Chi Zhang[1] | **Farzana R. Zaki**[1] | **Jungeun Won**[1,2] | **Stephen A. Boppart**[1,2,3,4,5,6]

[1]Beckman Institute for Advanced Science and Technology, University of Illinois Urbana-Champaign, Urbana, Illinois, USA

[2]Department of Bioengineering, University of Illinois Urbana-Champaign, Urbana, Illinois, USA

[3]Department of Electrical and Computer Engineering, University of Illinois Urbana-Champaign, Urbana, Illinois, USA

[4]Cancer Center at Illinois, University of Illinois Urbana-Champaign, Urbana, Illinois, USA

[5]Carle Illinois College of Medicine, University of Illinois Urbana-Champaign, Urbana, Illinois, USA

[6]NIH/NIBIB Center for Label-free Imaging and Multiscale Biophotonics (CLIMB), University of Illinois Urbana-Champaign, Urbana, Illinois, USA

Correspondence
Stephen A. Boppart, Beckman Institute for Advanced Science and Technology, University of Illinois Urbana-Champaign, Urbana, Illinois, USA.
Email: boppart@illinois.edu

Present address
Chi Zhang, Department of Chemistry, Purdue University, West Lafayette, Indiana, USA.

Funding information
GSK Center for Optical Molecular Imaging at the University of Illinois Urbana-Champaign; National Institutes of Health, Grant/Award Numbers: P41EB031772, R01CA241618, R01EB023232, R01CA213149, R01EB028615; National Science Foundation, Grant/Award Number: CBET 18-41539

Abstract

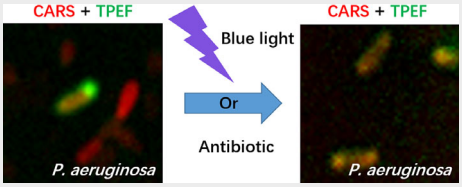

Pseudomonas aeruginosa (*P. aeruginosa*) is a multidrug-resistant human pathogen involved in numerous infections. Understanding the response of *P. aeruginosa* to various treatments is critical to developing new ways for the antimicrobial susceptibly test and more effective treatment methods. Conventional antimicrobial susceptibility tests lack molecular information at the single bacterium level. In this study, we used label-free multimodal nonlinear optical microscopy to identify an autofluorescence signal from pyoverdine, a siderophore of the bacteria, for quantification of *P. aeruginosa* responses to antibiotics and blue light treatment. We also discovered that the bleaching of the pyoverdine autofluorescence signals is correlated with the inactivation of *P. aeruginosa* and is perhaps one of the mechanisms involved in the blue light inactivation of *P. aeruginosa*.

KEYWORDS

blue light, coherent anti-Stokes Raman scattering, nonlinear optical imaging, *Pseudomonas aeruginosa*, two-photon excitation fluorescence

1 | INTRODUCTION

Pseudomonas aeruginosa (*P. aeruginosa*) is a gram-negative, rod-shaped bacterium that can cause pneumonia, septic shock, urinary and gastrointestinal tract infections, as well as skin and ear infections [1, 2]. It has a natural resistance to many antimicrobial drugs and can develop biofilms to protect itself from antibiotic treatment [3–5]. With the overuse of antibiotics and the lack of new antibiotic drug development over the past few decades, effective treatment of *P. aeruginosa* has become increasingly challenging for public health. Recent advances in several directions have encouraged the pharmaceutical industry to address the escalating crisis.

The first needed advancement is to develop efficient and accurate antimicrobial susceptibility tests for various clinical microbiology and pharmaceutic applications. Conventional methods to test the efficacy of an antimicrobial drug involve the spread plate method [6, 7], in which the bacteria are usually cultured for 24 h or longer to compare the colony-forming units or the size of zone-of-clearing. This method is easy to conduct but requires a longer incubation time for bacteria to grow, especially for bacteria samples obtained from patients that are more sensitive to environmental conditions. Additionally, the spread plate method lacks molecular information and single-cell resolution to understand treatment/resistant mechanisms at the single-bacterium level. Therefore, it is critical to develop new techniques for rapid evaluation of the antimicrobial susceptibility of drugs to the bacteria and molecular insights at the single-cell level. Several new approaches have been implemented to speed up the antimicrobial susceptibility test (AST) to a few hours [8–10] or even within 30 min [11]. Recently developed stimulated Raman scattering microscopy, when combined with isotope metabolite feeding, was shown to rapidly detect antibiotic responses of multiple bacteria within one cell cycle [12, 13], however with high instrument cost and sophisticated procedures. Nevertheless, optical microscopy methods can significantly shorten the time required for AST while offering rich chemical information about single bacterial cells.

The second advancement is to develop new treatment methods for bacteria with improved antimicrobial efficacy. Among the newly developed methods, phototherapy has gained increasing attention due to its high effectiveness, easy delivery, high penetration, and minimal side effects [14, 15]. For example, blue light is one of the most recognized spectral ranges of wavelengths for the treatment of various bacterial infections. Blue light at 400 nm can inactivate *P. aeruginosa* [16–18], *Enterobacteriaceae* [19], and other bacteria [20]. Blue light is also potentially effective in treating ear and skin infections [21, 22]. Methicillin-resistant *Staphylococcus aureus* can be effectively treated using 470 nm wavelength irradiation [23] and H_2O_2 treatment [24, 25]. Although the efficacy of blue light treatment of many bacteria strains is well appreciated, the mechanisms behind blue light bacterial inactivation are still elusive. Therefore, it is necessary to understand the interaction of blue light with the bacteria and how it affects the metabolism of bacteria on the molecular level with high resolution. Optical microscopy, being able to offer single-cell images with molecular contrasts, becomes an ideal candidate to address this need.

In this work, we used autofluorescence signals from *P. aeruginosa* as an optical signature to evaluate the bacterial response to treatment methods including antibiotics and blue light. According to our observations, autofluorescence signal intensities in the 450 nm fluorescence channel generated by the siderophore pyoverdine can be correlated with treatment time. Additionally, we revealed that pyoverdine molecules in *P. aeruginosa* can be bleached by either two-photon absorption of 800 nm femtosecond laser pulses or single-photon absorption of 405 nm blue light. This process is correlated with bacterial inactivation. This study sheds new light on the molecular-level understanding of the responses of *P. aeruginosa* to antibiotics and blue light using optical signatures from the bacteria.

2 | RESULTS

2.1 | Optical signatures of *P. aeruginosa* to antibiotic treatment

To explore the optical signatures of *P. aeruginosa*, we designed a multimodal nonlinear optical microscope that allows simultaneous acquisition of coherent anti-Stokes Raman scattering (CARS) and two-photon excitation fluorescence (TPEF) signals at 450 nm from bacteria cells. The microscopy system has been reported in a previous publication [26]. A description of the microscope can be found in Section 4.1 and a schematic is shown in Figure S1.

We first compared CARS and TPEF signals from antibiotic-treated and untreated (control) *P. aeruginosa*. Planktonic bacteria cells were treated with 60 μg/mL penicillin and 50 μg/mL streptomycin for 24 h before imaging. The antibiotic treatment effectively inactivated bacterial populations and slowed down the growth of bacteria. From Figure 1A–E, we found that although the CARS signals from bacteria cells did not show noticeable differences, the TPEF signals from antibiotic-treated bacteria decreased significantly. In Figure 1A,C, the TPEF

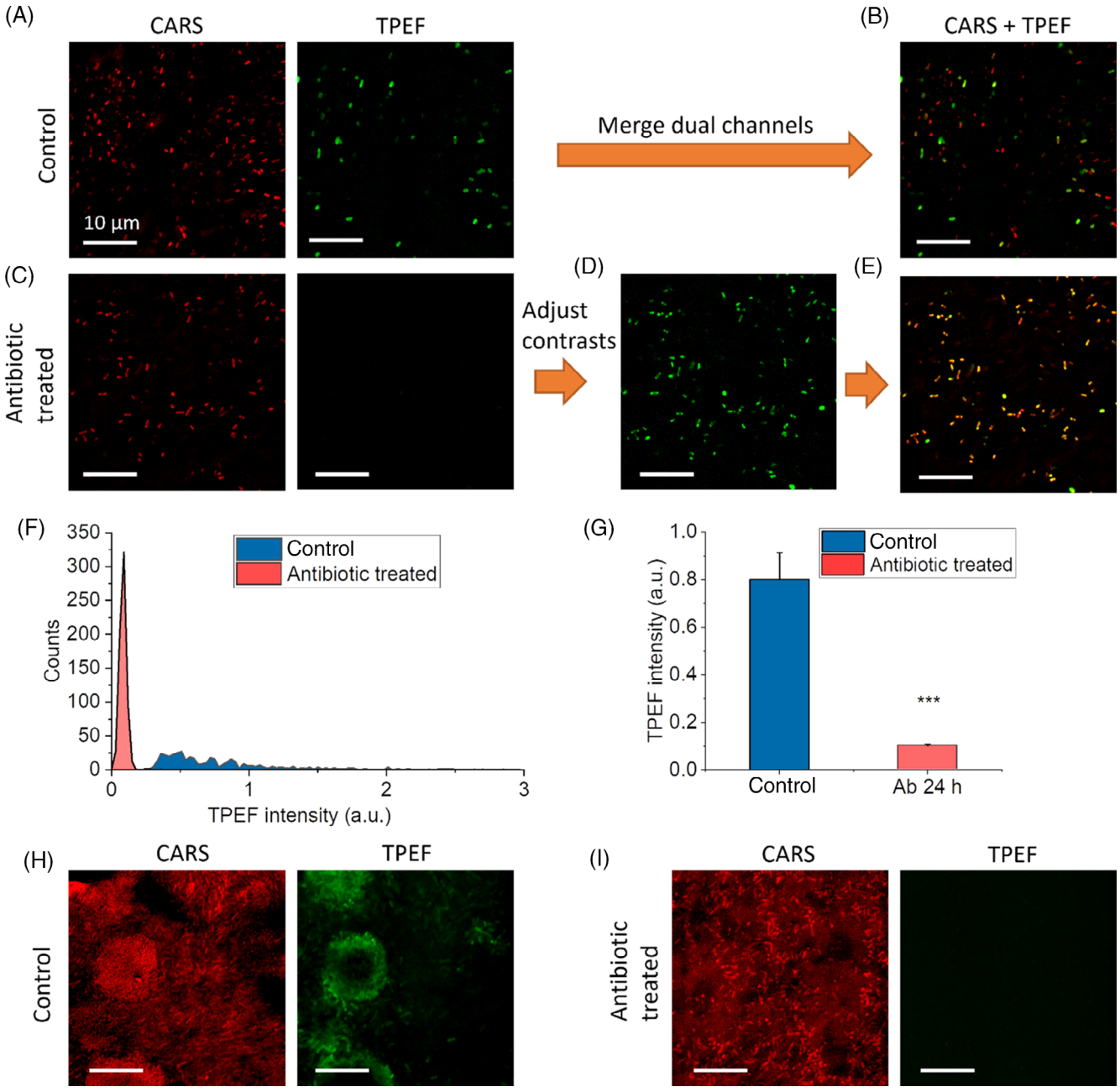

FIGURE 1 Autofluorescence signals from the treated and untreated bacteria. (A) CARS and TPEF images of untreated *P. aeruginosa*. (B) Merged CARS and TPEF channels from images in panel (A). (C) CARS and TPEF images of 24 h antibiotic-treated *P. aeruginosa*. (D) TPEF image in panel (C) after contrast adjustment. (E) Merged CARS and contrast-adjusted TPEF images of antibiotic-treated *P. aeruginosa*. (F) TPEF intensity histogram of the treated and untreated *P. aeruginosa*. (G) Average TPEF intensity of the treated and untreated *P. aeruginosa*. (H) CARS and TPEF images of untreated *P. aeruginosa* biofilm. (I) CARS and TPEF images of 24 h antibiotic-treated *P. aeruginosa* biofilm. The scale bar in (A) applies to all images. ***$p < 0.005$.

images are displayed at the same intensity scale. The intensity scale was adjusted to visualize the weak TPEF signals after the antibiotic treatment, as shown in Figure 1D. Figure 1F plots histograms of the averaged TPEF intensity from single bacteria cells. Figure 1G compares the average TPEF intensities from bacteria cells in the untreated (control) and antibiotic-treated conditions, which confirms the reduction of TPEF intensity as an optical signature of the antibiotic response of *P. aeruginosa*.

We also grew *P. aeruginosa* biofilms and investigated the optical signals of the bacteria cells residing in the biofilms. Figure 1H shows the untreated *P. aeruginosa* biofilm, where bacteria cells form clusters and display heterogeneous TPEF signal intensities within the cluster. The cells

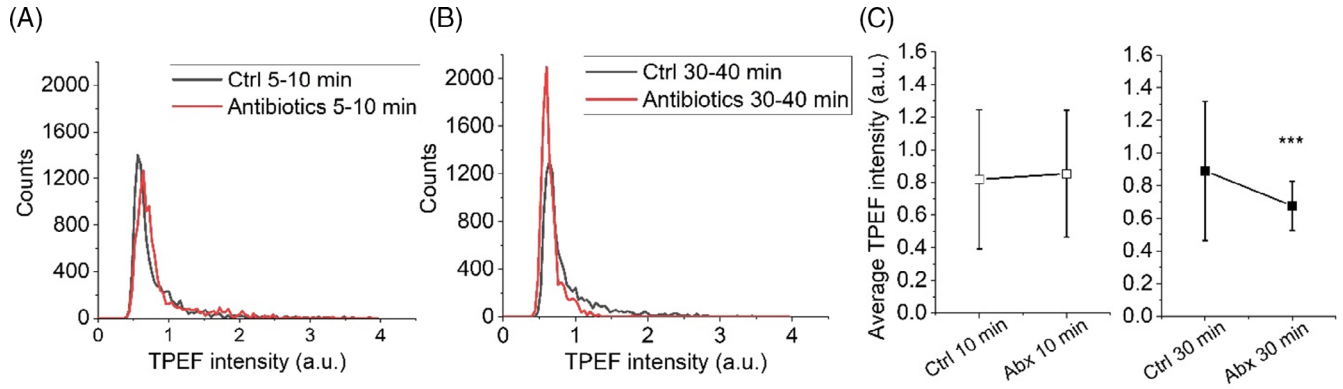

FIGURE 2 *P. aeruginosa* TPEF signals in response to antibiotic treatment. (A) Histograms of bacteria cell TPEF intensities for the untreated (control, ctrl) and 5–10 min antibiotic-treated groups. (B) Histograms of bacteria cell TPEF intensities for the untreated and 30–40 min antibiotic-treated groups. (C) Average intensities of *P. aeruginosa* TPEF signals for different treatment time. ***$p < 0.005$.

at the inner cores of the aggregations showed very low TPEF signals in the 450 nm channel, while the cells at the periphery part of the colony generated strong TPEF signals, suggesting higher metabolic activities at the outer regions of the colony. For the antibiotic-treated *P. aeruginosa* biofilm, we did not observe cell clusters. The TPEF signals in the 450 nm channel were also much weaker compared to the untreated biofilm, as shown in Figure 1I.

This decrease in autofluorescence signal can be used as an optical signature to rapidly assess the antibiotic response of *P. aeruginosa*. We monitored the TPEF signals from the *P. aeruginosa* cells after 5–10 and 30–40 min of antibiotic treatment. Figure 2A,B shows histograms of TPEF signals from bacteria cells. Next, Figure 2C compares the average intensity values for different treatment durations. The results indicated a statistically significant reduction of TPEF signal intensity after antibiotic treatment of 30–40 min.

2.2 | Understanding the origin of the optical signature

To further understand the TPEF signals generated by *P. aeruginosa*, we magnified and overlaid CARS and TPEF images. Figure 3A displays the CARS, TPEF, and superimposed images from the untreated *P. aeruginosa*. We found that the CARS signals and the strong TPEF signals from the 450 nm channel did not overlap. However, after antibiotic treatment, although the overall TPEF signal intensity decreased, the CARS and TPEF signals perfectly co-localized and showed in yellow due to the combination of the red CARS and green TPEF pseudo-colors, as shown in Figure 3B. This feature suggests that TPEF signals at 450 nm are likely generated from different molecules before and after the antibiotic treatment. Furthermore, the intensity distribution of TPEF signals inside the bacteria cells before the antibiotic treatment manifests strong signals at the edges of many cells, as shown in Figure 3C–E. This indicates the molecules that generate the TPEF signal are likely located within or near the cell walls. Moreover, some cells have a 'dot-like structure' with strong TPEF signals in the 450 nm channel inside the cells. This observation agrees with many other reports, and these features are likely siderosomes that are linked to pyoverdine synthesis [27–29]. Pyoverdine is a siderophore produced by *P. aeruginosa* and can help bacteria cells to chelate iron ions from the environment [5]. It has an absorption band at ~400 nm and has a fluorescence emission signal in the 400–500 nm range [30, 31]. *P. aeruginosa* produces pyoverdine and trafficks it to and along the bacteria cell walls, or enriches it within the siderosomes, or secretes it to the environment [32–34]. These features and pathways agree well with our observations in the 450 nm fluorescence channel. Therefore, we hypothesize that pyoverdine contributes to the strong fluorescence signals in the TPEF 450 nm channel for untreated *P. aeruginosa*. After treatment, the TPEF signals are much weaker and colocalized with most of the CARS signals. We believe such signals are majorly contributed by nicotinamide adenine dinucleotide hydrogen (NADH) which has an emission maximum around 450 nm [35–37]. Compared to pyoverdine, NADH has a much smaller two-photon absorption cross-section and weaker fluorescence emission [38]. The CARS signals are primarily from proteins in cells. Before treatment, the accumulation of pyoverdine in sidersomes that have lower protein concentration results in the spatial separation of TEPF and CARS signals. After treatment, the remaining NADH mostly overlaps with cellular proteins, giving co-localized TPEF and CARS signals.

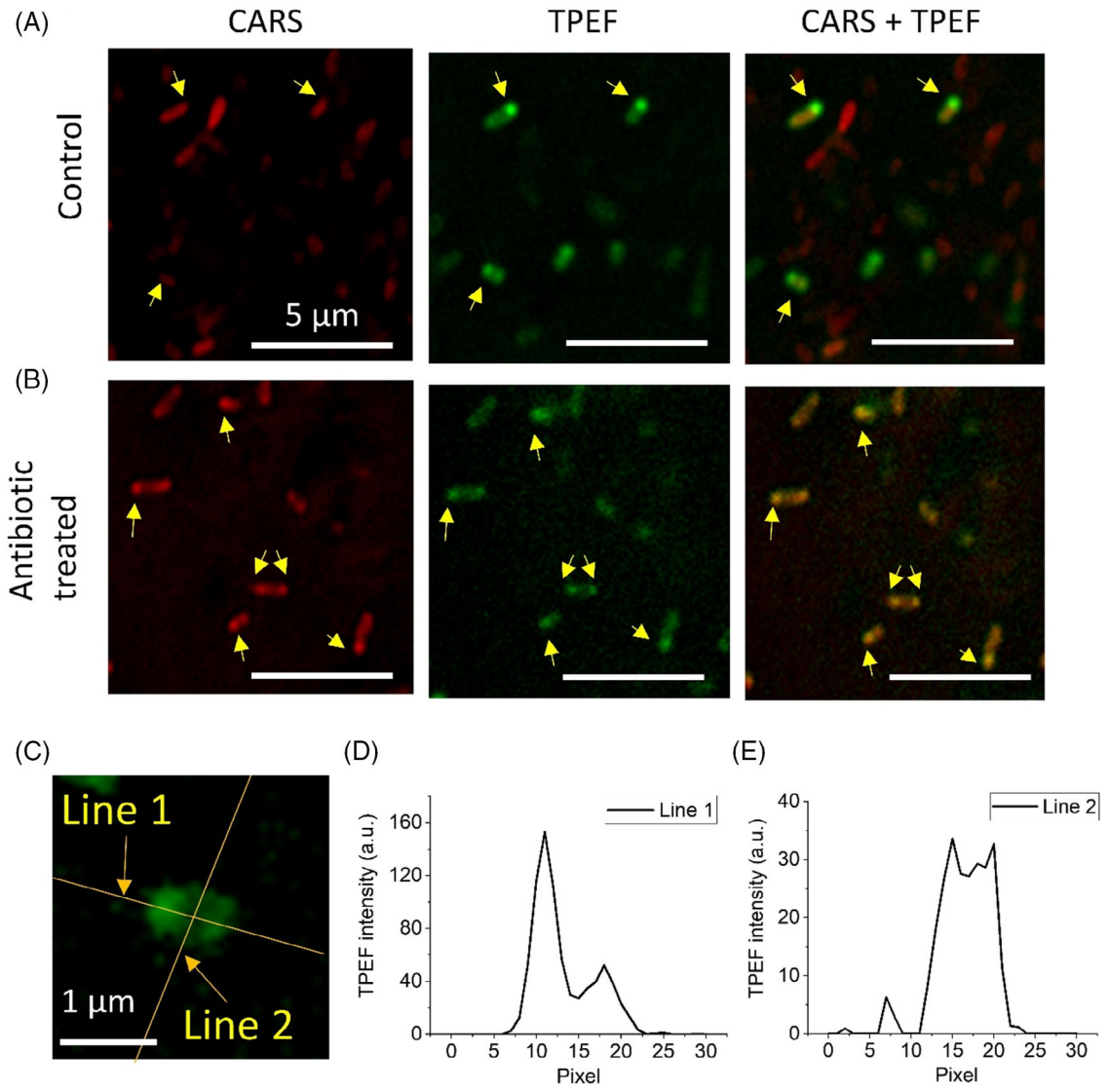

FIGURE 3 Localization of the TPEF signals in *P. aeruginosa*. (A) CARS, TPEF, and the combined images of the bacteria cells for the control group. (B) CARS, TPEF, and the combined images of the bacteria cells for the 24-h antibiotic-treatment group. (C) Magnified TPEF image of a *P. aeruginosa* cell from the control group. (D) and (E) Intensity profiles along line 1 and line 2 in panel (C), respectively.

To validate this hypothesis, we measured the UV–VIS spectrum from the bacteria and compared the results with a pure pyoverdine solution. As shown in Figure 4A, the pyoverdine molecule has a strong absorption band at ~400 nm, which can also be found in the *P. aeruginosa* solution, though at much weaker signal intensities. Furthermore, we noticed that the *P. aeruginosa* in our culture conditions did not produce pyocyanin, another fluorescent molecule with absorption peaks at 380 nm and 700 nm [39]. Pyoverdine-mutant bacteria were used to further confirm the pyoverdine production by *P. aeruginosa*. We compared the parent (PAO) and pyoverdine-mutant strains (pvdA and pvdD mutants). The pvdA and pvdD genes encode ornithine hydroxylase and non-ribosomal peptide synthetase related to pyoverdine synthesis in *P. aeruginosa* [32, 40]. The parent strain showed a strong absorption peak at ~400 nm from the background removed UV–VIS spectra, while the pyoverdine mutant strains lacked this UV–VIS signature peak (Figure 4B).

Furthermore, a drop of planktonic bacterial solution from each sample was inoculated onto agar plates, incubated for 12 h of growth, and illuminated with blue light for fluorescence excitation. The PAO strain shows a very strong fluorescence signal, while the mutant strains are non-fluorescent (Figure 4C). Figure 4D shows CARS and TPEF images of the PAO and two mutant strains, from which much weaker TPEF signals were visible from the images of the pvdA and pvdD mutant bacteria. Figure 4E quantifies the fluorescence intensities in the TPEF

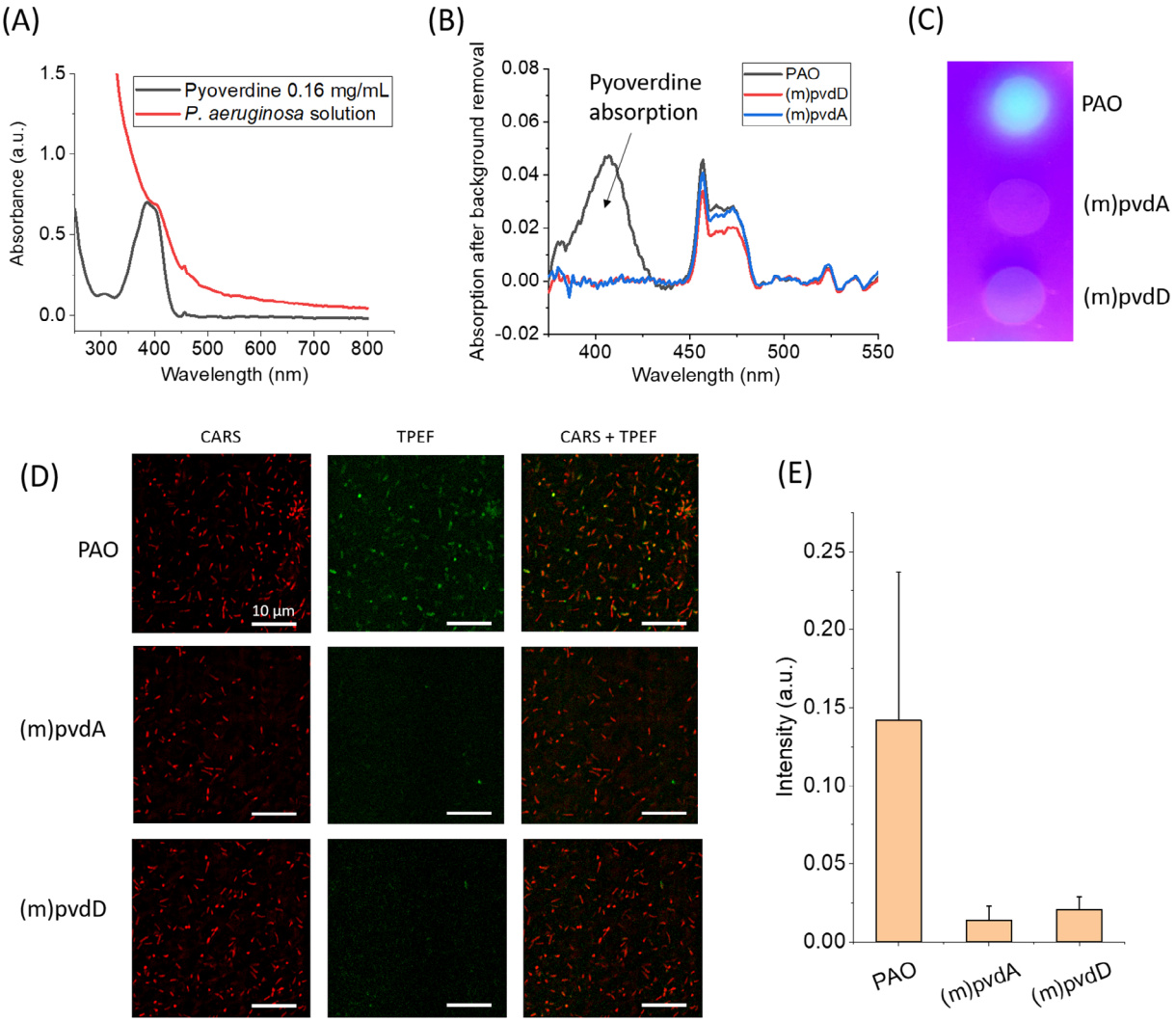

FIGURE 4 Absorption and autofluorescence properties of *P. aeruginosa* and the pyoverdine mutant bacteria strains. (A) UV–VIS spectra of the pure pyoverdine at 0.16 mg/mL (black) and the *P. aeruginosa* solution (red). (B) UV–VIS spectra of the PAO (black), pvdA mutant (blue), and pvdD mutant (red) groups after background slope subtraction. (C) A photo showing the autofluorescence signals from the PAO, pvdA mutant, and pvdD mutant groups under blue light illumination. (D) CARS, TPEF, and combined images of three *P. aeruginosa* strains. (E) Average TPEF intensities of the three bacteria samples.

channels in Figure 4D. Collectively, these results indicate that pyoverdine contributes to the strong autofluorescence signals detected in the 450 nm TPEF channels before the antibiotic treatment.

2.3 | Blue light responses of *P. aeruginosa*

Besides generating strong autofluorescence signals in the 450 nm channel, we observed photobleaching of pyoverdine by the 800 nm femtosecond laser continuous exposure. Figure 5A displays time-lapse TPEF images of *P. aeruginosa* cells. Cells with a strong TPEF signal in the 450 nm channel showed a significant signal decrease after continuous imaging, while the cells with low TPEF signals exhibited stable signals after the same exposure time (Figure 5B). Video S1 shows the photobleaching of the autofluorescence signals during imaging. This observation suggests that pyoverdine molecules, which produce strong autofluorescence signals, are likely bleached by the two-photon absorption of the 800 nm pulses. Since NADH molecules also have autofluorescence signals in the 450 nm region and usually do not have rapid photobleaching in this laser power range, the weak TPEF autofluorescence signals from cells are attributed to NADH. Another possible origin of the weak autofluorescence signal is from pyoverdine molecules that are away from the focal plane, which would experience much less two-photon absorption-induced photobleaching.

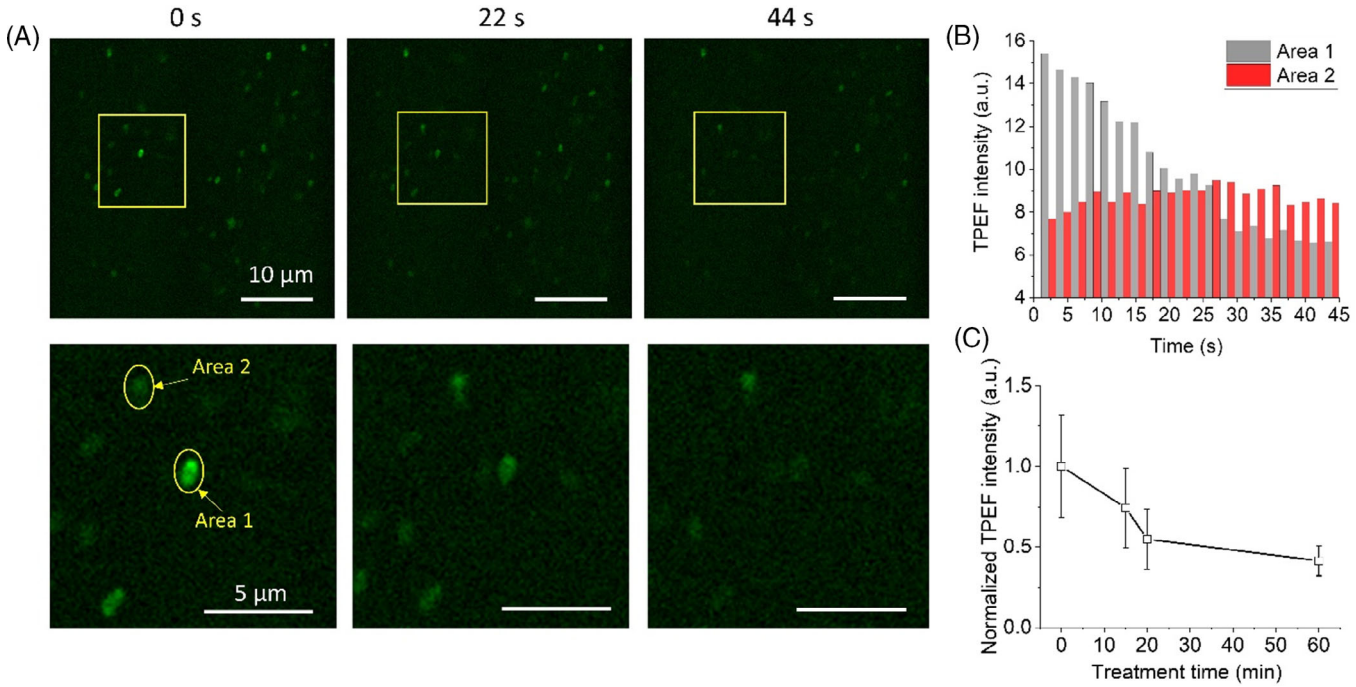

FIGURE 5 Photobleaching of TPEF signals in *P. aeruginosa*. (A) Time-lapse TPEF images of bacteria cells using the 800 and 1040 nm laser beams for excitation. The top row is the large field-of-view while the bottom row shows magnified areas in corresponding squares from the top row. (B) Averaged TPEF intensities as a function of imaging time selected from two areas in panel (A). (C) Normalized, averaged TPEF signal from *P. aeruginosa* after 40 mW blue light treatment for different treatment time lengths.

Blue light has been reported as an effective phototherapy method to inactivate *P. aeruginosa* [16, 18]. Since two-photon absorption of 800 nm laser pulses can photobleach the strong pyoverdine autofluorescence signals of *P. aeruginosa*, we hypothesize that 400 nm blue light would have a similar effect on pyoverdine photobleaching. We designed a blue light treatment device as shown in Figure S2. This device uses a 405 nm LED and can focus the light onto a 10 × 10 mm^2 area. The maximum output of the LED is 1 W, while the maximum light intensity at focus on the sample is 200 mW. We treated 200 μL of planktonic *P. aeruginosa* in a 1.5 mL microcentrifuge tube by directly exposing the sample under the blue light for different time durations and observed the decrease of autofluorescence signal from *P. aeruginosa* at 450 nm as a function of treatment duration (Figure 5C). The decrease in averaged autofluorescence signals suggests that autofluorescence molecules in *P. aeruginosa* are photobleached by the 405 nm blue light. Note that due to the differences in light source and beam size, LED blue light treatment results in a much slower photobleaching effect compared to laser scanning of the femtosecond lasers. A much higher energy density of femtosecond laser pulses gives a faster photobleaching effect compared to the blue LED treatment.

Next, we studied the efficacy of blue light inactivation on *P. aeruginosa*. An illustration of the experimental procedure in treating bacteria cells is shown in Figure 6A. We dispensed 200 μL of planktonic *P. aeruginosa* in brain heart infusion (BHI) broth media and treated the bacteria with 0.2 W/cm^2 for different time durations. Then, a drop of bacteria solution was placed on an agar plate and incubated for 5 h. The results showed that blue light treatment of 15 min can effectively inactivate the *P. aeruginosa* (Figure 6A). To further evaluate the treatment efficacy of blue light for pre-grown bacteria, we designed a new 3D method based on the vertical penetration of bacteria through polyethylene filters (Figure 6B). *P. aeruginosa* was first cultured on agar plates for 24 h before being treated with blue light for different time durations. Then, filters removed from filtered pipette tips were placed on the treated surfaces for 20 h of growth. Active bacteria can penetrate through the filter better. After removal of the filters followed by 20 h of growth, we illuminated the filters under the blue light source and compared the penetration depth of the bacteria into the filters by measuring the fluorescence signals from the bacteria. As shown in Figure 6B, the blue light after a 10-min exposure can reduce the penetration of *P. aeruginosa* into the filter; the extended light treatment of 15 min or longer can further inactivate the *P. aeruginosa* grown on agar.

Using the method described in Figure 6A, we compared the effect of blue light treatment for the PAO and pyoverdine mutant strains. The averaged bacterial

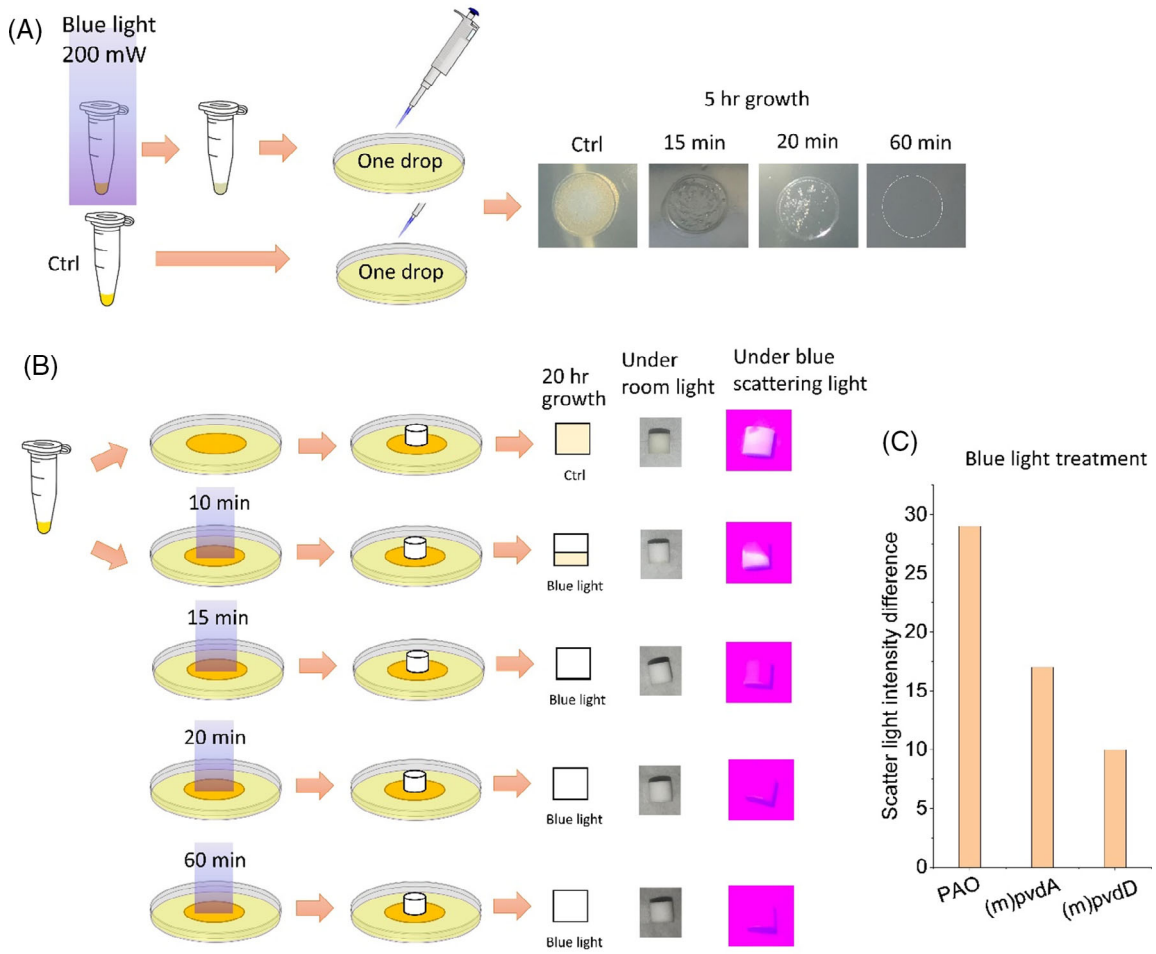

FIGURE 6 Blue light treatment of bacteria and proposed evaluation method for efficacy. (A) Illustration of the blue light treatment method for *P. aeruginosa* solutions (left) and treatment results using 200 mW blue light (right). The treatment was performed for 15, 20, and 60 min. The bacteria were allowed to grow for 5 hr on agar plates. For the photo taken from the 60 min treatment, a circle was drawn on the photo to show the drop location. Each drop contained 10 μL bacteria solution. (B) Illustration of the blue light treatment method for *P. aeruginosa* pre-grown bacteria colonies on agar plates. (left) and the treatment results (right). Photos were taken under both room light and blue scattering light. (C) Bacteria growth inhibition for the PAO, pvdA mutant, and pvdD mutant groups. The scattered light intensity was used to quantify the bacteria growth.

intensity variations (scattering signal collected by a camera) are compared in Figure 6C. A more effective inactivation and reduced bacteria growth were found for the PAO strain, giving less light scattering under room light. We found that the PAO strain, which produces pyoverdine, is more vulnerable to blue light treatment than the pyoverdine mutant strains. This suggests that bleaching of pyoverdine by blue light is one of the mechanisms for *P. aeruginosa* inactivation.

3 | DISCUSSION

From label-free nonlinear optical imaging of treated and untreated (control) *P. aeruginosa* cells, we discovered a 450 nm autofluorescence signal as an optical signature to rapidly evaluate bacteria responses to antibiotic and blue light treatments. Our studies show that this optical signature is likely associated with the presence of pyoverdine, a siderophore responsible for iron chelating. Pyoverdine has been identified as a potential target for reducing the virulence of *P. aeruginosa* [41, 42]. We revealed antibiotic-reducing and blue-light-bleaching effects on pyoverdine. We found that pyoverdine bleaching by blue light is likely associated with blue light-based bacteria inactivation since the pyoverdine-producing bacteria strain is more susceptible to blue light treatment compared to the pyoverdine mutant strains. Our findings help to better illustrate mechanisms behind inactivation processes and to design better ways for more effective treatment.

P. aeruginosa can also produce pyocyanin, a blue toxin associated with biofilm formation [43, 44]. This molecule also generates fluorescence signals in the 450 nm channel [45]. However, we did not detect

measurable pyocyanin production from our bacteria strains, which was confirmed by the UV–VIS spectra. Pyocyanin is usually produced in the later stage of *P. aeruginosa* growth. In this study, the bacteria were cultured and harvested for imaging within the first 48 h. The production of pyocyanin and pyoverdine share the same precursor [46]. Therefore, in later stages, the increased pyocyanin production is possibly linked to reduced pyoverdine generation by the cells. Further studies on the correlations between the two autofluorescence molecules will be carried out in the future.

The methods presented in this study rely on the siderophore autofluorescence signals from *P. aeruginosa*. One limitation is that they do not apply to nonfluorescent bacteria. However, many clinically important bacteria are fluorescent [47], making the methods demonstrated in this work applicable in these conditions. In addition, although this research is mostly focused on fluorescence signal characterization, the CARS microscopy feature can potentially aid in understanding the bacteria responses to treatment, similar to what has been presented for stimulated Raman scattering microscopy [12, 13]. Other nonlinear optical imaging modalities such as transient absorption microscopy can also be integrated to further understand bacterial pigments [24].

4 | MATERIALS AND METHOD

4.1 | Nonlinear optical microscope

Both CARS and TPEF imaging were performed on a lab-built multimodal nonlinear optical microscope. Briefly, a tunable femtosecond laser (Chameleon Discovery, Coherent) output a fixed 1040 nm laser beam and a frequency tunable laser beam. We set the tunable wavelength to 800 nm as the pump and applied the fixed wavelength at 1040 nm as the Stokes to excite the C-H Raman transition for CARS imaging. The combined laser beams were sent to a 2D galvo-scanner (Cambridge Technology) for 2D beam scanning. A 60× water immersion objective lens (UPlanApo 60×, NA = 1.2) was used for laser focusing. The resolution of the CARS and TPEF microscope was ∼300 nm. The CARS signals were detected using a photomultiplier tube (PMT) (H7422-40, Hamamatsu) in the forward direction. The filter for rejecting input laser beams and fluorescence signals for CARS imaging was a narrow bandpass filter (650/13 nm, FF01-650/13/25, Semrock). The TPEF signals were acquired in the epi-direction using a second identical PMT. The dichroic mirror for signal separation had a cut-off wavelength of 785 nm (Di02-R785-25x36, Semrock). The filter for TPEF signal selection was a bandpass filter centered at 450 nm (FF01-451/106-25, Semorck). Signals from the PMTs were amplified and inverted by a pre-amplifier (PMT-4V3, Advanced Research Instruments Corp.) for each channel. The amplified signals were then acquired by a high-speed data acquisition card (PCIe-6351, National Instruments). The image acquisition and laser scanning were controlled by LabVIEW-based software.

Both 800 and 1040 nm laser pulses were used for non-degenerate TPEF excitation and simultaneous CARS imaging. Both laser pulses were ∼ 150 fs and ∼20 mW at the sample and were scanned at a pixel dwell time of 10 μs. Note that continuous imaging of the nontreated cells with this laser power can result in the photobleaching of pyoverdine autofluorescence signals. Images acquired in Figures 1–4 were acquired in the first frame of laser scanning. For the photobleaching using femtosecond lasers, the same laser power and pixel dwell time were used. Continuous laser scanning and signal acquisition were performed for 45 s.

4.2 | Image analyses

Image analyses were performed using ImageJ. Raw images were saved as .txt files, mainly containing 400 × 400 pixels. CARS and TPEF images were displayed in pseudo colors for better demonstration. Merging image channels, plotting image line profiles, and particle analysis were performed using ImageJ functions. Time-lapse TPEF images showing photobleaching of pyoverdine in bacteria cells were collected continuously at 2.2 s per frame, and selected frames are displayed in Figure 5.

4.3 | *P. aeruginosa* cultures and mutant strains

P. aeruginosa was purchased from ATCC (ATCC 14203) and was cultured in brain heart infusion (BHI) broth (BD 237500, Fisher Scientific) and on agar (BD 241830, Fisher Scientific), following the protocol provided by the manufacturer. BHI broth was prepared by mixing 18.5 g of the BHI powder with 0.5 L of distilled (DI) water and autoclaving the solution at 250 °F for 15 min. BHI agar was prepared by mixing 26 g of dehydrated BHI agar powder with 500 mL of DI water while heating (180 °F) and stirring to obtain a suspension having a final pH of 7.3. The BHI agar solution was then autoclaved at 250 °F for 15 min, cooled, and poured into different Petri dishes. BHI agar plates were checked for visual contamination before use. *P. aeruginosa* bacteria were streaked on agar plates and incubated at 37°C under 5% CO_2.

Planktonic *P. aeruginosa* cultures were prepared following the overnight growth of bacteria colonies on BHI

agar. An inoculation loop was used to remove a single *P. aeruginosa* colony from the agar plate, which was then seeded into a conical tube with 10 mL BHI media, allowing for growth over 24 h at 37°C inside an incubator before being prepared for imaging or treatment. *P. aeruginosa* biofilms were prepared using the same bacterial suspension, diluted in fresh BHI media (5 mL) at a 1:6 volumetric ratio. This solution was then incubated at 37°C for different time durations with a maximum of 48 h. Next, the biofilm mass was transferred into culture dishes or glass coverslips for treatment and imaging.

The PAO, pvdA mutant (PA2386, lacZbp01q2E02), and pvdD mutant (PA2399, lacZbp02q4E07) *P. aeruginosa* strains were obtained from the Manoil Lab *P. aeruginosa* Mutant Library [48, 49]. The strains were cultured similarly using the previously mentioned methods. UV–VIS spectra were measured using a commercially available spectrophotometer (GeneQuant 100, Biochrom) and disposable UV-transparent cuvettes.

4.4 | Antibiotic and blue light treatments

Penicillin–streptomycin (100×, containing 6 mg/mL penicillin and 5 mg/mL streptomycin) was purchased from ThermoFisher Scientific. For treatment of 24 h duration, a 1× concentration of the antibiotics was used. For treatment performed in Figure 2, a 100× concentration of the antibiotics was applied. A blue LED with a 1 W output was purchased from Thorlabs (M405L4, Thorlabs) and powered by an LED driver (LEDD1B, Thorlabs). The driver controlled the output power of the LED. The irradiance of the incident light on the surface was 0.04–0.2 W/cm^2, based on the optical beam area of 1 cm^2. The cells were treated for different time lengths (10–60 min) to monitor the changes in autofluorescence signals. The spectrum of the LED was measured by a spectrum analyzer (OSA201C, Thorlabs). Two lenses (AC254-035-A-ML and AC254-040-A-ML) were used to focus the LED light onto a 10 mm × 10 mm square area for treatment.

4.5 | Photos from bacteria samples

Photos from bacteria samples after growth were taken with a CCD camera with a fixed background. For the autofluorescence images, the samples were illuminated under the blue LED after removing the lenses. The photos were taken without the ambient light present. ImageJ was also used to perform the analysis of the photos. Images for comparison were all taken at the same time in the same ambient light environment.

AUTHOR CONTRIBUTIONS

Chi Zhang, Jungeun Won, and Stephen A. Boppart designed research. Chi Zhang carried out imaging experiments and data analysis. Farzana R. Zaki and Jungeun Won prepared bacteria and biofilm samples. Jungeun Won and Chi Zhang performed UV–VIS measurements. Chi Zhang, Farzana R. Zaki, and Stephen A. Boppart wrote the paper. Stephen A. Boppart obtained funding for the research.

ACKNOWLEDGMENTS

The authors want to thank GlaxoSmithKline for the sponsored research and equipment support of the GSK Center for Optical Molecular Imaging at the University of Illinois Urbana-Champaign. This research was also financially supported in part by grants from the National Institutes of Health (R01CA241618, R01EB023232, P41EB031772, R01CA213149, and R01EB028615) and the National Science Foundation (CBET 18-41539). Additional information can be found at http://biophotonics.illinois.edu.

CONFLICT OF INTEREST STATEMENT

Stephen Boppart is a co-founder of LiveBx, Champaign, IL, which is licensing intellectual property from the University of Illinois Urbana-Champaign to develop novel optical sources and label-free multimodal multiphoton imaging platforms for biological and medical applications. Chi Zhang declares no competing interests.

DATA AVAILABILITY STATEMENT

The data that support the findings of this study are available from the corresponding author upon reasonable request and through a collaborative research agreement.

ORCID

Chi Zhang https://orcid.org/0000-0002-7735-5614
Jungeun Won https://orcid.org/0000-0003-1007-4049
Stephen A. Boppart https://orcid.org/0000-0002-9386-5630

REFERENCES

[1] G. P. Bodey, R. Bolivar, V. Fainstein, L. Jadeja, *Rev. Infect. Dis.* **1983**, *5*, 279.
[2] K. G. Kerr, A. M. Snelling, *J. Hosp. Infection* **2009**, *73*, 338.
[3] K. Poole, *Front. Microbiol.* **2011**, *2*, 65.
[4] Z. Pang, R. Raudonis, B. R. Glick, T.-J. Lin, Z. Cheng, *Biotechnol. Adv.* **2019**, *37*, 177.
[5] E. Banin, M. L. Vasil, E. P. Greenberg, *Proc. Natl. Acad. Sci.* **2005**, *102*, 11076.
[6] S. Puttaswamy, S. Gupta, H. Regunath, L. Smith, S. Sengupta, *Arch. Clin. Microbiol.* **2018**, *9*, 3.
[7] N. Ncube, A. Afolayan, A. Okoh, *Afr. J. Biotechnol.* **2008**, *7*, 1797.
[8] J. Choi, J. Yoo, M. Lee, E.-G. Kim, J. S. Lee, S. Lee, S. Joo, S. H. Song, E.-C. Kim, J. C. Lee, H. C. Kim, Y.-G. Jung, S. Kwon, *Sci. Transl. Med.* **2014**, *6*, 267ra174.

[9] J. Choi, H. Y. Jeong, G. Y. Lee, S. Han, S. Han, B. Jin, T. Lim, S. Kim, D. Y. Kim, H. C. Kim, E.-C. Kim, S. H. Song, T. S. Kim, S. Kwon, *Sci. Rep.* **2017**, *7*, 1.
[10] H. Sun, C. W. Chan, Y. Wang, X. Yao, X. Mu, X. Lu, J. Zhou, Z. Cai, K. Ren, *Lab Chip* **2019**, *19*, 2915.
[11] D. C. Spencer, T. F. Paton, K. T. Mulroney, T. J. J. Inglis, J. M. Sutton, H. Morgan, *Nat. Commun.* **2020**, *11*, 5328.
[12] M. Zhang, W. Hong, N. S. Abutaleb, J. Li, P.-T. Dong, C. Zong, P. Wang, M. N. Seleem, J.-X. Cheng, *Adv. Sci.* **2020**, *7*, 2001452.
[13] W. Hong, C. W. Karanja, N. S. Abutaleb, W. Younis, X. Zhang, M. N. Seleem, J. X. Cheng, *Anal. Chem.* **2018**, *90*, 3737.
[14] A. Lipovsky, Y. Nitzan, A. Gedanken, R. Lubart, *Lasers Surg. Med.* **2010**, *42*, 467.
[15] F. F. Sperandio, Y.-Y. Huang, M. R. Hamblin, *Recent Pat. Anti-Infect. Drug Discovery* **2013**, *8*, 108.
[16] G. Fila, A. Kawiak, M. S. Grinholc, *Virulence* **2017**, *8*, 938.
[17] J. S. Guffey, J. Wilborn, *Photomed. Laser Therapy* **2006**, *24*, 680.
[18] T. Dai, A. Gupta, Y. Y. Huang, R. Yin, C. K. Murray, M. S. Vrahas, M. E. Sherwood, G. P. Tegos, M. R. Hamblin, *Antimicrob. Agents Chemother.* **2013**, *57*, 1238.
[19] F. D. Halstead, Z. Ahmed, J. R. Bishop, B. A. Oppenheim, *Antimicrobial Resistance Infect. Control* **2019**, *8*, 1.
[20] M. Hirose, Y. Yoshida, K. Horii, Y. Hasegawa, Y. Shibuya, *Arch. Oral Biol.* **2021**, *122*, 105024.
[21] S. L. White, US Patent 8,021,405. **2011**.
[22] T. Dai, A. Gupta, Y. Y. Huang, M. E. Sherwood, C. K. Murray, M. S. Vrahas, T. Kielian, M. R. Hamblin, *Photomed. Laser Surg.* **2013**, *31*, 531.
[23] C. S. Enwemeka, D. Williams, S. K. Enwemeka, S. Hollosi, D. Yens, *Photomed. Laser Surg.* **2009**, *27*, 221.
[24] P. T. Dong, H. Mohammad, J. Hui, L. G. Leanse, J. Li, L. Liang, T. Dai, M. N. Seleem, J.-X. Cheng, *Adv. Sci.* **2019**, *6*, 1900030.
[25] J. Hui, P.-T. Dong, L. Liang, T. Mandal, J. Li, E. R. Ulloa, Y. Zhan, S. Jusuf, C. Zong, M. N. Seleem, G. Y. Liu, Q. Cui, J.-X. Cheng, *Adv. Sci.* **2020**, *7*, 1903117.
[26] C. Zhang, S. A. Boppart, *Anal. Chem.* **2020**, *92*, 15943.
[27] F. Imperi, P. Visca, *FEBS Lett.* **2013**, *587*, 3387.
[28] O. Cunrath, V. Gasser, F. Hoegy, C. Reimmann, L. Guillon, I. J. Schalk, *Environ. Microbiol.* **2015**, *17*, 171.
[29] L. Guillon, S. Altenburger, P. L. Graumann, I. J. Schalk, *PLoS One* **2013**, *8*, e79111.
[30] D. Kang, N. V. Kirienko, *Pathogens* **2021**, *10*, 9.
[31] J. Greenwald, F. Hoegy, M. Nader, L. Journet, G. L. A. Mislin, P. L. Graumann, I. J. Schalk, *J. Biol. Chem.* **2007**, *282*, 2987.
[32] M. T. Ringel, T. Brüser, *Microbial Cell* **2018**, *5*, 424.
[33] A. Bonneau, B. Roche, I. J. Schalk, *Sci. Rep.* **2020**, *10*, 1.
[34] W.-J. Chen, T.-Y. Kuo, F.-C. Hsieh, P.-Y. Chen, C.-S. Wang, Y.-L. Shih, Y.-M. Lai, J.-R. Liu, Y.-L. Yang, M.-C. Shih, *Sci. Rep.* **2016**, *6*, 1.
[35] C. Zhang, S. A. Boppart, *Sci. Rep.* **2021**, *11*, 6671.
[36] A. Alex, E. J. Chaney, M. Žurauskas, J. M. Criley, D. R. Spillman Jr., P. B. Hutchison, J. Li, M. Marjanovic, S. Frey, Z. Arp, S. A. Boppart, *Exp. Dermatol.* **2020**, *29*, 953.
[37] G. A. Snyder, S. Kumar, G. K. Lewis, K. Ray, *Front. Immunol.* **2023**, *14*, 1213180.
[38] Y. Qin, Y. Xia, *Front. Phys.* **2021**, *9*, 642302.
[39] G. Bodelón, V. Montes-García, V. López-Puente, E. H. Hill, C. Hamon, M. N. Sanz-Ortiz, S. Rodal-Cedeira, C. Costas, S. Celiksoy, I. Pérez-Juste, L. Scarabelli, A. la Porta, J. Pérez-Juste, I. Pastoriza-Santos, L. M. Liz-Marzán, *Nat. Mater.* **2016**, *15*, 1203.
[40] V. Gasser, M. Malrieu, A. Forster, Y. Mély, I. J. Schalk, J. Godet, *Q. Rev. Biophys.* **2020**, *53*, e1.
[41] D. R. Kirienko, D. Kang, N. V. Kirienko, *Front. Microbiol.* **2019**, *9*, 3317.
[42] D. Kang, A. V. Revtovich, A. E. Deyanov, N. V. Kirienko, *mSphere* **2021**, *6*, e0040121.
[43] G. W. Lau, D. J. Hassett, H. Ran, F. Kong, *Trends Mol. Med.* **2004**, *10*, 599.
[44] S. J. H. Sui, R. Lo, A. R. Fernandes, M. D. G. Caulfield, J. A. Lerman, L. Xie, P. E. Bourne, D. L. Baillie, F. S. L. Brinkman, *Int. J. Antimicrob. Agents* **2012**, *40*, 246.
[45] T. Das, A. I. Ibugo, W. Klare, M. Manefield, *Microbial Biofilms-Importance Appl.* **2016**, *13*, 23.
[46] A. Price-Whelan, L. E. Dietrich, D. K. Newman, *Nat. Chem. Biol.* **2006**, *2*, 71.
[47] M. Y. Rennie, D. Dunham, L. Lindvere-Teene, R. Raizman, R. Hill, R. Linden, *Diagnostics* **2019**, *9*, 22.
[48] M. A. Jacobs, A. Alwood, I. Thaipisuttikul, D. Spencer, E. Haugen, S. Ernst, O. Will, R. Kaul, C. Raymond, R. Levy, L. Chun-Rong, D. Guenthner, D. Bovee, M. V. Olson, C. Manoil, *Proc. Natl. Acad. Sci.* **2003**, *100*, 14339.
[49] K. Held, E. Ramage, M. Jacobs, L. Gallagher, C. Manoil, *J. Bacteriol.* **2012**, *194*, 6387.

SUPPORTING INFORMATION

Additional supporting information can be found online in the Supporting Information section at the end of this article.

How to cite this article: C. Zhang, F. R. Zaki, J. Won, S. A. Boppart, *J. Biophotonics* **2024**, *17*(3), e202300384. https://doi.org/10.1002/jbio.202300384